Journal of The Electrochemical Society

OPEN ACCESS

Stabilizing $NaCrO_2$ by Sodium Site Doping with Calcium

To cite this article: Lituo Zheng *et al* 2019 *J. Electrochem. Soc.* **166** A2058

Stabilizing $NaCrO_2$ by Sodium Site Doping with Calcium

Lituo Zheng,[1,*] J. C. Bennett,[2] and M. N. Obrovac[1,3,,z]**

[1] *Department of Chemistry, Dalhousie University, Halifax, N.S. B3H 4R2, Canada*
[2] *Department of Physics, Acadia University, Wolfville, N.S. B4P 2R6, Canada*
[3] *Department of Physics and Atmospheric Science, Dalhousie University, Halifax, N.S. B3H 4R2, Canada*

Layered cathode materials based on abundant, low cost raw materials have garnered interest in recent years. O3-type $NaCrO_2$ is a promising cathode material as it offers decent energy density and is easy to synthesize. In this study, calcium doped $NaCrO_2$ was synthesized using a solid-state method and the resulting $[Na_{1-2x}Ca_x]CrO_2$ materials were studied in sodium cells. Compared to calcium-free $NaCrO_2$, $[Na_{0.9}Ca_{0.05}]CrO_2$ has improved capacity retention without sacrificing reversible capacity. The enhanced performance was ascribed to structural stabilization of $NaCrO_2$ by Ca-doping, as observed by ex-situ X-ray diffraction. Finally, calcium doped $NaCrO_2$ was also found to have improved air-stability than the pristine material.

 [DOI: 10.1149/2.1041910jes]

Manuscript submitted May 7, 2019; revised manuscript received June 3, 2019. Published June 14, 2019.

Due to the potential lithium scarcity, sodium ion batteries are receiving significant attention from researchers as a possible alternative technology for electric vehicles and grid energy storage.[1,2] In recent years the development of sodium ion batteries has largely followed the footprints of lithium ion batteries.[3] For example, carbonaceous anode materials and carbonate-based organic electrolyte have been commonly studied.[4–7] Among many candidates for cathode materials, layered sodium transition metal oxides have been the focus of research as they are characteristic of having high energy density, stable structures, and facile syntheses. Specifically, cobalt-free cathode materials are attractive due to the high price and toxicity of cobalt.[3,8–10]

O3-type $NaCrO_2$ has a relatively high average voltage and good energy density among all sodium transition metal oxides.[11,12] Moreover, Xia et al. showed that $NaCrO_2$ has great thermal stability and there is virtually no reactivity between desodiated $Na_{0.5}CrO_2$ and non-aqueous electrolyte up to 350°C.[13] They attributed the lack of exothermic behavior to the minimal oxygen release of $Na_{0.5}CrO_2$.[13] Hatchard et al. demonstrated a high coulombic efficiency of 99.97% for $NaCrO_2$/$NaCrO_2$ symmetric cells, the highest coulombic efficiency reported so far for sodium ion batteries materials.[7] Interestingly, the lithium counterpart of $NaCrO_2$, $LiCrO_2$, is inactive in lithium cells, despite their compositional and structural similarities.[14] This phenomenon is attributed to the different sizes of the interstitial spaces in $NaCrO_2$ and $LiCrO_2$ structures. The irreversible migration of chromium ions into the tetrahedral sites in the lithium layer of $LiCrO_2$ causes it to become inactive after the first charge.[14] Such migration is less favorable for $Na_{1-x}CrO_2$ when $x \leq 0.5$ due to the larger tetrahedral sites in $NaCrO_2$.[15,16] Further removal of sodium ($x > 0.5$) also makes it gradually become inactive.[15,16] Therefore, previous work limited the desodiation process to $Na_{1-x}CrO_2$ ($x = \sim 0.5$) in order for $NaCrO_2$ to cycle well.[11,12] A capacity fade of ~20% in 50 cycles is usually observed for $NaCrO_2$ in organic solvents.[12,17,18] Some research regarding improving the capacity retention of $NaCrO_2$ has been published. Ding et al. and Yu et al. reported carbon coated $NaCrO_2$ with enhanced cycling performance.[12,17] Tsuchiya et al. used ballmilling and reheating to introduce more grain boundaries in $NaCrO_2$. They demonstrated that the enriched grain boundaries could suppress the O3-P3 phase transition, resulting in better cyclability.[18]

While substantial work on sodium layered oxides so far has been conducted on transition metal layer doping, there have been few reports on sodium layer doping.[19–22] Cation mixing in the alkaline metal layer is well known to be detrimental to battery performance, with the classic example of Li/Ni mixing in cathode materials for lithium ion batteries.[23] Due to the blocked alkaline ion diffusion pathways, cation mixing results in decreased capacity and increased hysteresis, and is usually to be avoided.[14,24] Recently, Matsui et al. and Han et al. reported the structure and electrochemistry of calcium substituted P2-Na_xCoO_2.[25,26] The ionic radius of calcium (~1 Å) is similar to that of sodium (~1.03 Å) and is significantly larger than most first row transition metals (0.5–0.7 Å). Therefore, it is energetically more favorable for calcium to occupy sites in the sodium layers, compared to the transition metal layers. P2-Na_xCoO_2 is known for its step-like profiles in voltage versus capacities plots, due to sodium/vacancy ordering during the (de)intercalation of sodium. Calcium substitution was reported to hinder such ordering, leading to smoothed voltage curves and improved cyclability, at the expense of a slight loss of capacity.[25,26] The strategy of using sodium site substitution is attractive and presents opportunities for the development of new sodium cathode materials. In this study, $[Na_{1-2x}Ca_x]CrO_2$ was synthesized and characterized for the first time. It is shown that calcium doping $NaCrO_2$ not only improves its cycling performance, but also surprisingly enhances its air-stability.

Experimental

Compositions in the $[Na_{1-2x}Ca_x]CrO_2$ series were prepared by mixing stoichiometric quantities of Na_2CO_3 (99.0%, Sigma Aldrich), CaO (99.9%, Sigma Aldrich), and Cr_2O_3 (98.0%, Sigma Aldrich) using a SPEX 8000 mill. Generally, four 7/16" stainless steel balls and ~6 g of powders were milled for one hour in air. The resulting powders were then pressed into pellets and heated under flowing Ar (with an upstream Ti sponge) at 900°C for 3 hours. Samples were then quenched to room temperature and transferred to Ar-filled glove box without air exposure.

Electrode preparation was carried out in an Ar-filled glove box. Slurries were made by mixing active material, PVDF binder (HSV 900, KYNAR), and carbon black (Imerys Graphite and Carbon) in an 8:1:1 weight ratio with an appropriate amount of N-methyl-2-pyrrolidone (Sigma Aldrich, anhydrous 99.5%). These components were mixed with two 0.5" tungsten carbide balls in a Retsch PM200 rotary mill (100 rpm, 1 hour) to create a uniform slurry. Typically, ~0.4 g of active material was used for making slurry. The slurry was then coated onto aluminum foil with a coating bar having a 0.15 mm gap and dried under vacuum at 80°C overnight. The resulting electrode coatings had active loadings of 1–2 mg/cm^2. Circular electrodes were punched from the coating and incorporated into 2325-type coin cells in an Ar-filled glove box. Na disks punched from thin foil (~0.4 mm) rolled from sodium ingot (Sigma Aldrich, ACS reagent grade) were used as counter/reference electrodes. Two Celgard 2300 and one blown microfiber separator (3M Company) were used as separators. 1 M $NaClO_4$ (Aldrich, 98%) in propylene carbonate (PC, BASF) with 2%

*Electrochemical Society Student Member.
**Electrochemical Society Member.
zE-mail: mnobrovac@dal.ca

monofluoroethylene carbonate (FEC, BASF) was used as electrolyte. Cells were cycled with a Maccor Series 4000 Automated Test System (Maccor Inc., Tulsa OK). The ambient cycling temperature was 30.0°C (±0.1°C).

X-ray diffraction (XRD) measurements were made using a Rigaku Ultima IV Diffractometer equipped with a Cu anode X-ray tube, a scintillation detector, and a diffracted beam monochromator. All samples were loaded into a gastight sample holder (DPM Solutions) in argon atmosphere for XRD measurements. For ex-situ measurements, coin cells cycled to different cutoff voltages were stopped and opened in an Ar-filled glove box. The electrodes were recovered from the cells and rinsed with dimethyl carbonate (DMC, battery grade, BASF) several times. The recovered materials were then transferred to a zero-background silicon wafer and sealed in the gastight sample holder for the ex situ XRD measurements. Scanning electron microscope (SEM) measurements were performed using a field emission scanning electron microscope (TESCAN MIRA 3). Transmission electron microscopy (TEM) images were taken using a Philips CM30 electron microscope equipped with energy-dispersive X-ray spectroscopy (EDS). TEM sample powders were sonicated for 5 minutes in hexane and then dropped onto a TEM carbon coated grid for measurements.

Results and Discussion

Figure 1 shows XRD patterns of the synthesized $[Na_{1-2x}Ca_x]CrO_2$ samples. Phase-pure samples with an O3 structure were obtained for $x \leq 0.05$. For samples with $x \geq 0.07$, $CaCr_2O_4$ and Cr_2O_3 impurities become visible in the XRD profiles, as shown in Figure 1b. This indicates a limited solid solution range under the synthesis conditions used here. Rietveld refinements were performed on phase-pure samples with $x \leq 0.05$. The O3-type α-$NaFeO_2$ structure was used for the refinements. In initial refinements Na and Cr were allowed to mix, however this resulted in a negative occupancy of Na/Cr in Cr/Na sites. The same phenomenon was observed when Ca and Cr were allowed to mix. This indicates the large size difference between Na/Ca and Cr tends to make cation mixing unfavorable. This suggests that calcium ions are only located in sodium sites, consistent with previous studies of calcium doped Na_xCoO_2. Therefore cation mixing was not considered in the final refinements. Reasonably good fits with Bragg R values less than 5 were obtained for calcium-substituted samples. An example of a refined pattern is shown in Figure 1c for the composition with $x = 0.05$. Previous studies have shown that dopant may cause a reduction in the grain size of the O3 phase when transition metal is doped into $NaCrO_2$.[27] It is also believed that the improved cyclability of transition metal doped $NaCrO_2$ may be a consequence of reduced grain size.[27] Such phenomenon is not observed in this study as the compounds synthesized in the $[Na_{1-2x}Ca_x]CrO_2$ ($x \leq 0.05$) series have identical grain sizes (~30 nm) as calculated from XRD patterns.

Figures 2a–2b shows SEM images of $NaCrO_2$ and $[Na_{0.9}Ca_{0.05}]CrO_2$. Both materials consist of ~300 nm plates with hexagonal morphology. There are no observable impurity phases in the SEM images. Figures 2c–2d shows TEM images and corresponding selected area electron diffraction (SAED) patterns of $NaCrO_2$ and $[Na_{0.9}Ca_{0.05}]CrO_2$. The electron diffraction patterns indicate the crystal structures are similar for both samples. The hexagonally arranged diffraction spots in the [001] zone axis SAED patterns for both samples may be indexed according to the O3 structure (R-3m). EDS analyses were also conducted on individual platelet crystallites. For $[Na_{0.9}Ca_{0.05}]CrO_2$, 10 randomly selected particles had the same Ca/Cr ratio (~0.05). It is therefore reasonable to conclude that the composition of the crystallite platelets is fairly homogeneous.

It has been reported that $NaCrO_2$ can be cycled with good reversibility with an upper cutoff voltage of 3.6 V.[14] Cycling beyond this point causes significant irreversible capacity and poor cyclability.[15,16] This is also demonstrated in Figure 3, where the voltage-capacity curve of $NaCrO_2$ and $[Na_{0.9}Ca_{0.05}]CrO_2$ cycled in different voltage ranges are shown. When cycled between 2 V–3.6 V, $NaCrO_2$ has a reversible capacity of 120 mAh/g and an irreversible capacity less than 10 mAh/g.

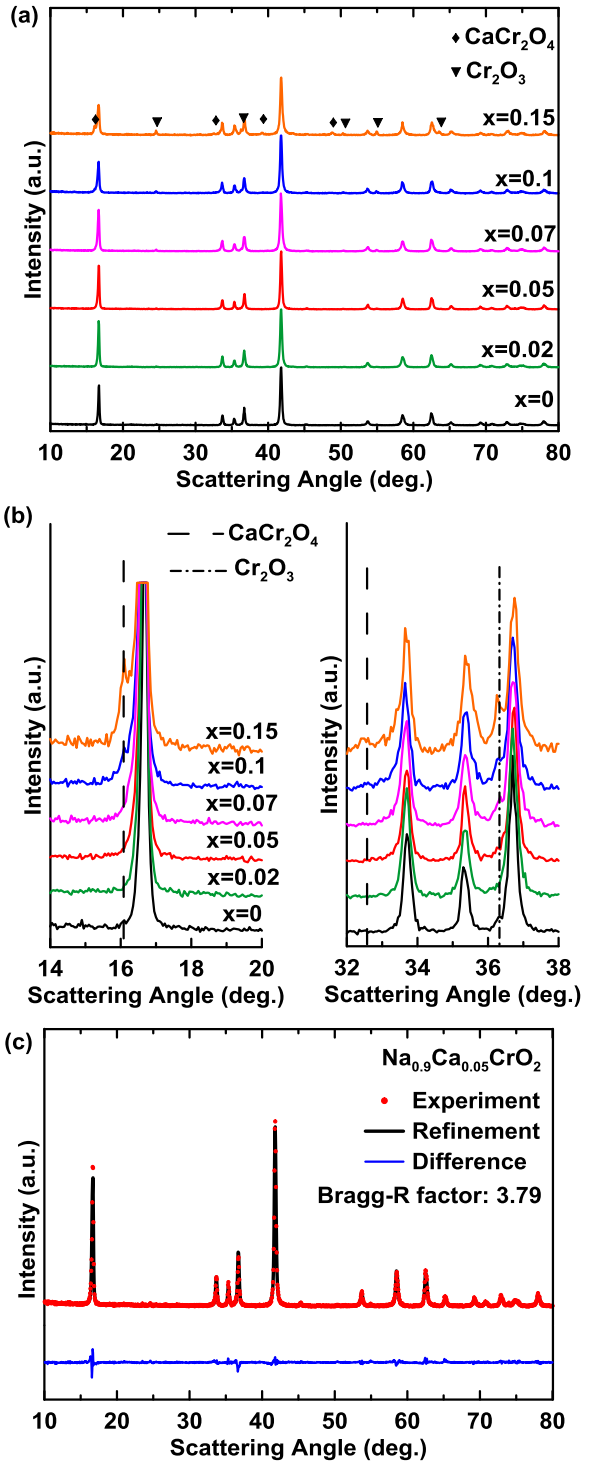

Figure 1. (a) XRD patterns of the synthesized $Na_{1-2x}Ca_xCrO_2$ series with impurity phase peaks labeled as indicated. (b) Enlarged XRD patterns. (c) Rietveld refinement of $Na_{0.9}Ca_{0.05}CrO_2$.

When the cell was charged to 3.7 V, both reversible and irreversible capacities slightly increase. As the upper cutoff voltage increases to 3.8 V, an irreversible capacity of 100 mAh/g is obtained with large hysteresis. Further charging to 4 V, where almost all the sodium has been removed from the structure, results in significantly increased hysteresis and decreased capacity.

For $[Na_{0.9}Ca_{0.05}]CrO_2$, similar behavior can be observed when it is cycled between 2 V–3.6 V and 2 V–3.7 V. However, when cycled

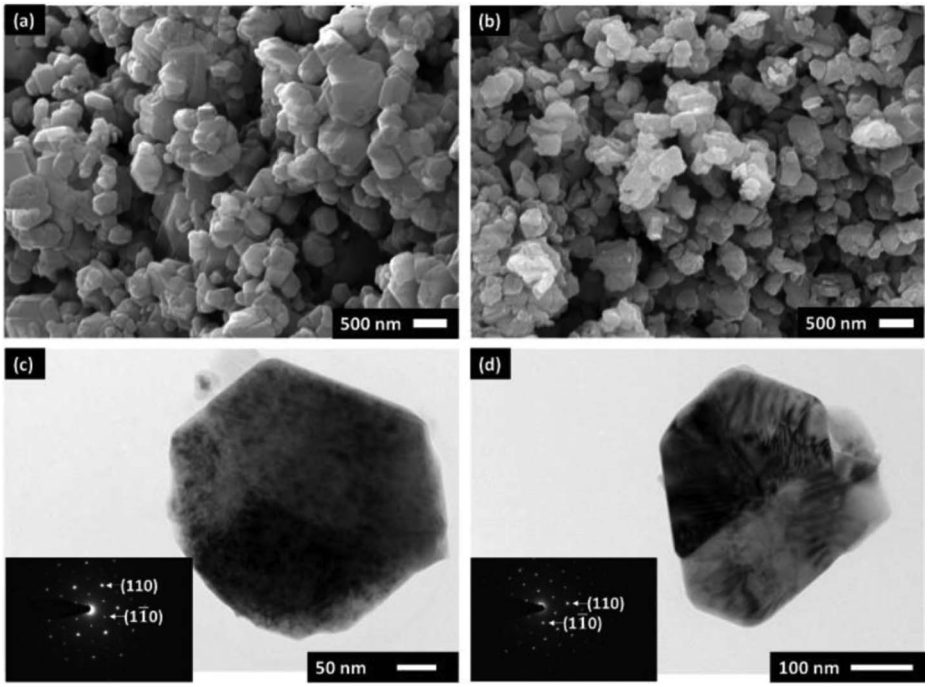

Figure 2. (a) SEM image of $NaCrO_2$. (b) SEM image of $Na_{0.9}Ca_{0.05}CrO_2$. (c) TEM image of $NaCrO_2$. (d) TEM image of $Na_{0.9}Ca_{0.05}CrO_2$.

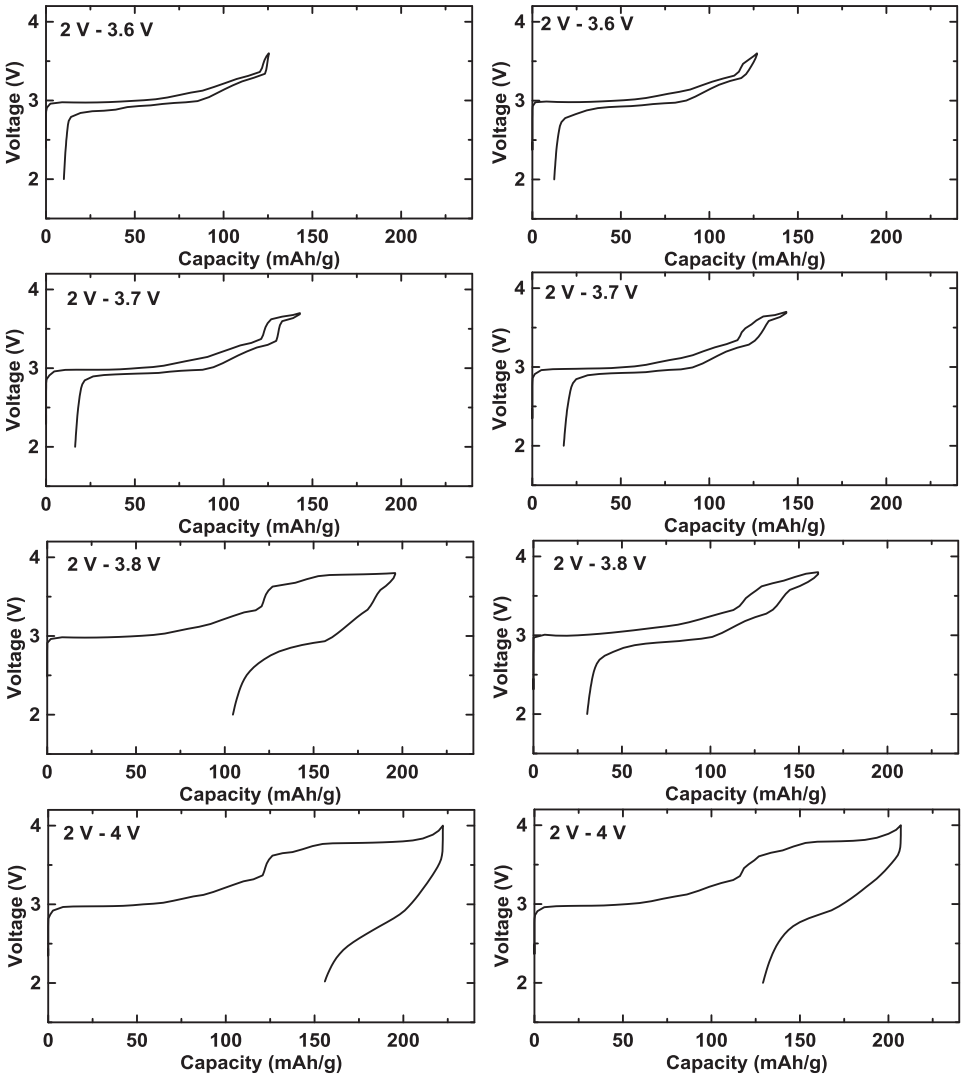

Figure 3. Voltage-capacity curve of $NaCrO_2$ (left) and $Na_{0.9}Ca_{0.05}CrO_2$ (right) in different voltage ranges.

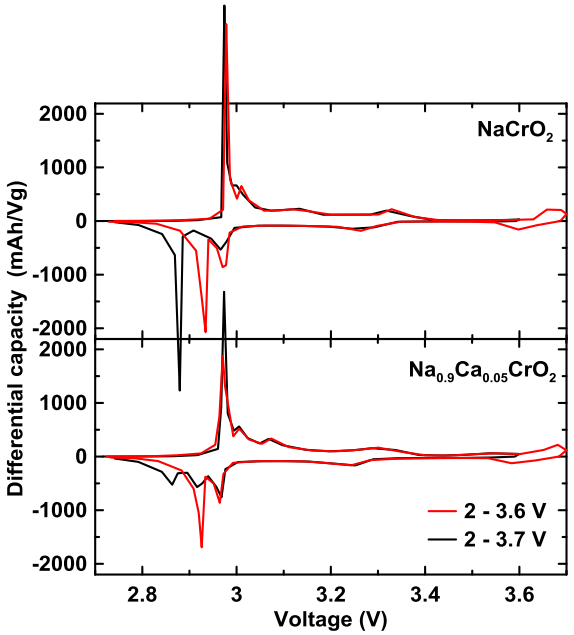

Figure 4. Differential capacity curve of $NaCrO_2$ and $Na_{0.9}Ca_{0.05}CrO_2$.

between 2 V–3.8 V and 2 V–4 V, $[Na_{0.9}Ca_{0.05}]CrO_2$ has higher reversible capacity and smaller hysteresis, compared to $NaCrO_2$ cycled in the same voltage range. The reason for this improvement is unclear. It is speculated that the reason for the improved cycling is that the calcium-substitution results in a more stable structure during sodium (de)intercalation, as will be shown below. It might also be possible that calcium prevents the migration of chromium ions into the sodium layer due to the stronger electrostatic repulsion resulting from the 2+ charge of the Ca^{2+} ion. The voltage curves of $[Na_{0.9}Ca_{0.05}]CrO_2$ also have less distinct plateaus compared to $NaCrO_2$. This can be easily seen in the differential capacity curves shown in Figure 4, where less intense and broader peaks are observed for $[Na_{0.9}Ca_{0.05}]CrO_2$. Therefore, the addition of Ca may help suppress ordering in the Na-layer or other phase transformations, which have been associated with fade.

Figures 5a–5b shows the cycling performance of $NaCrO_2$ and $[Na_{0.9}Ca_{0.05}]CrO_2$. After 50 cycles in the voltage range of 2 V–3.6 V, 83.0% of the initial capacity is retained for $NaCrO_2$. This number is consonant with other research.[12,17,18] When the cycling voltage range is increased to 2 V–3.7 V, the initial capacity is slightly increased, but capacity retention becomes worse, with only ~77.8% of the initial capacity remaining after 50 cycles. $[Na_{0.9}Ca_{0.05}]CrO_2$ has enhanced capacity retentions of 90.8% and 89.7% when cycled between 2 V–3.6 V and 2 V–3.7 V, respectively. Figures 5c–5d compares the long-term cyclability and coulombic efficiency of the two materials. Significant improvement can be observed for the calcium substituted sample. $Na_{0.9}Ca_{0.05}CrO_2$ retains 76.1% and 67.9% of its capacity after 500 cycles in the voltage range of 2 V–3.6 V and 2 V–3.7 V, while less than half of the initial capacity is retained for $NaCrO_2$ in both voltage ranges. The fade rate per cycle of $[Na_{0.9}Ca_{0.05}]CrO_2$ in the last 100 cycles is only 0.029%, compared to 0.082% for $NaCrO_2$. The coulombic efficiency of $[Na_{0.9}Ca_{0.05}]CrO_2$ (~99.8%) is also constantly higher than that of $NaCrO_2$ (~99.6%).

As immobile calcium in the sodium sites might hinder sodium diffusion, it is possible that the rate capability might be compromised by calcium doping. However, reports by Matsui et al. and Han et al. show that calcium substituted samples have rate capabilities at least as good as undoped samples.[25,26] Han et al. even showed that $[Na_{0.6}Ca_{0.07}]CoO_2$ displayed much better rate performance than $Na_{0.73}CoO_2$.[26] They attributed the improved rate performance to the more stable structure of $[Na_{0.6}Ca_{0.07}]CoO_2$, which facilitates sodium diffusion over the entire potential range. Figure 6 shows a

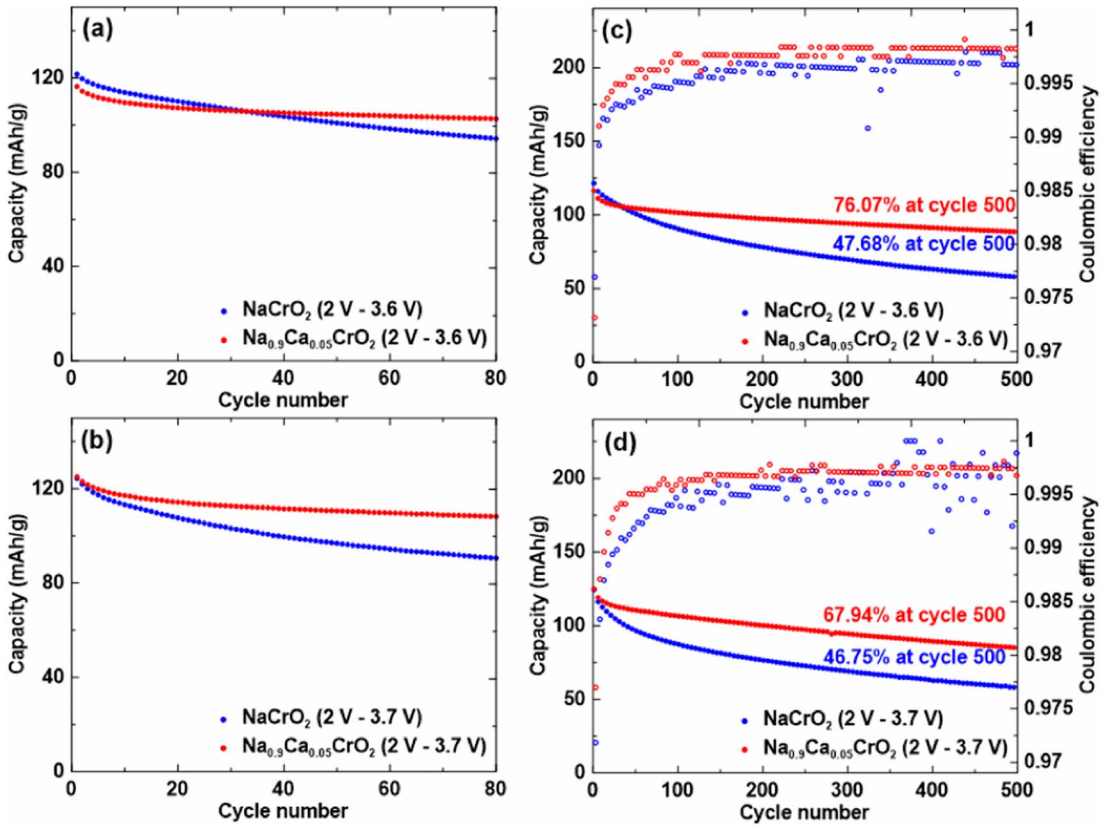

Figure 5. Discharge capacity and coulombic efficiency versus cycle number of $NaCrO_2$ and $Na_{0.9}Ca_{0.05}CrO_2$.

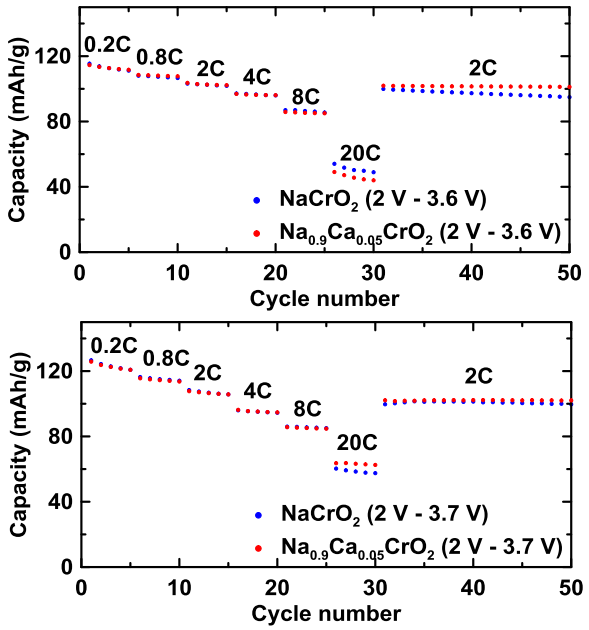

Figure 6. Discharge capacity of $NaCrO_2$ and $Na_{0.9}Ca_{0.05}CrO_2$ cycled at different C-rates.

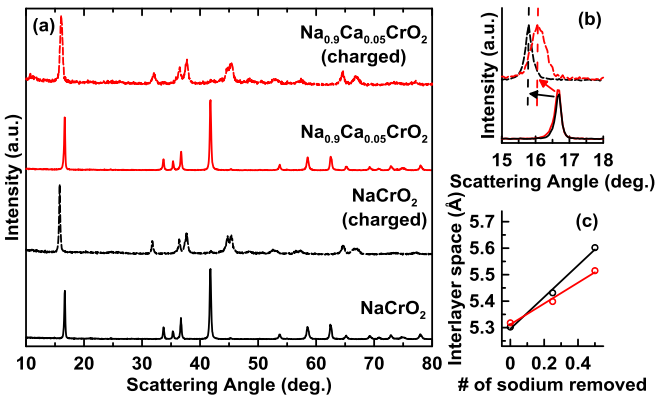

Figure 7. (a) Ex situ XRD patterns of $NaCrO_2$ and $Na_{0.9}Ca_{0.05}CrO_2$ after being charged to 3.6 V, compared to uncharged XRD patterns. (b) Enlarged XRD patterns showing the position change of (003) peak between 15° to 18°. (c) Calculated interlayer distance of $NaCrO_2$ and $Na_{0.9}Ca_{0.05}CrO_2$ during charging. Line styles in (b) and (c) are the same as used with each composition in (a).

comparison of the rate performance of $NaCrO_2$ and $[Na_{0.9}Ca_{0.05}]CrO_2$. Both $NaCrO_2$ and $Na_{0.9}Ca_{0.05}CrO_2$ have impressive rate performance. At a high current of 8C (1000 mA/g), both materials retain a capacity of more than 80 mAh/g. This indicates that a small amount of calcium doping does not deteriorate the rate capability. This result is in agreement with studies by Matsui et al. and Han et al. regarding calcium doped Na_xCoO_2.[25,26]

In order to understand the superior cycling performance of calcium-substituted $Na_{0.9}Ca_{0.05}CrO_2$, ex-situ XRD measurements were performed on both $NaCrO_2$ and $Na_{0.9}Ca_{0.05}CrO_2$. The results are compared in Figure 7. Figure 7a shows that both materials transition from an O3 to a P'3 phase when charged to 3.6 V. The shift of the (003) peaks of both materials to lower angle indicates an increase in interlayer distance during desodiation. This is due to a reduced screening effect of sodium between oxygen layers and a resulting stronger repulsion between alternating oxygen layers. Such anisotropic expansion/contraction along the *c* axis during cycling gradually causes irreversible structural changes and capacity fade.[28] A closer examination in Figure 7b shows that although both charged materials have the same phase behavior, the (003) peak shift during charging is less pronounced for $[Na_{0.9}Ca_{0.05}]CrO_2$ than $NaCrO_2$. This indicates a greater expansion of the interlayer distance in $NaCrO_2$ during charging, as shown in Figure 7c. It should be noted that the interlayer spacing of desodiated $Na_{0.5}CrO_2$ measured in this study (~5.6 Å) is consistent with previous studies.[11,15] It is believed the strong interaction between Ca^{2+} and O^{2-} leads to mitigated volume expansion, resulting in a more stable structure and improved cyclability. The peak broadening of desodiated $Na_{0.9}Ca_{0.05}CrO_2$ shown in Figure 7b might be caused by stacking faults due to the presence of calcium in partially desodiated layers.

Figure 8a shows ex-situ XRD profiles of $NaCrO_2$ and $[Na_{0.9}Ca_{0.05}]CrO_2$ electrodes in their fully discharged state after 50 cycles. Even though both cycled materials have similar O3-type XRD patterns, a careful examination shows that peak splitting can be observed in the XRD pattern of cycled $NaCrO_2$ but not for cycled $[Na_{0.9}Ca_{0.05}]CrO_2$. Some examples are shown in the enlarged XRD patterns in Figures 8b–8c for the (101), (102), and (104) diffraction lines. The peak splitting of $NaCrO_2$ after extensive cycling can be ascribed to the formation of the O'3 phase. According to other research, O3 phase $NaCrO_2$ starts to transition to O'3 phase once desodiation starts.[14,15] This result shows that the O3 structure of $[Na_{0.9}Ca_{0.05}]CrO_2$ is retained after 50 cycles, while the O3 structure of cycled $NaCrO_2$ is not completely recovered. The gradual phase transition of $NaCrO_2$ from the O3 to O'3 phase during cycling indicates a less stable structure, compared to $[Na_{0.9}Ca_{0.05}]CrO_2$.

It is well-known that most O3-type sodium cathode materials readily react with air.[29] Such behavior is typically accompanied by desodiation and/or the intercalation of water.[29,30] Air-sensitivity of cathode materials is one of the main obstacles that hinder the

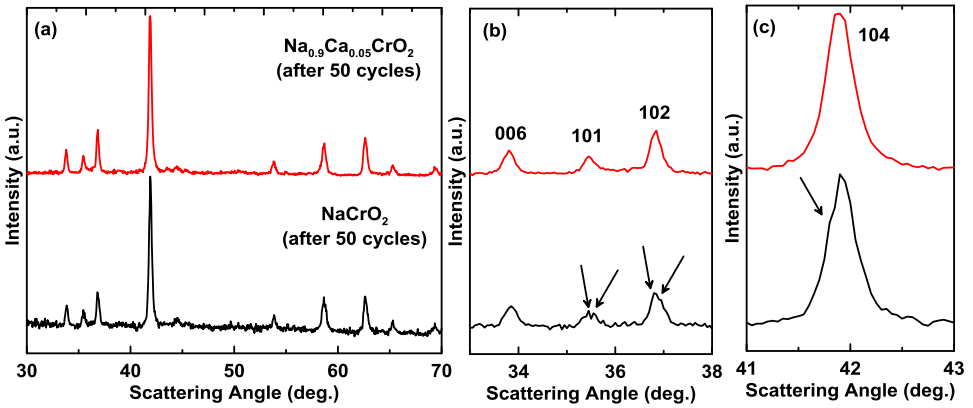

Figure 8. (a) Ex situ XRD patterns of $NaCrO_2$ and $Na_{0.9}Ca_{0.05}CrO_2$ electrodes after 50 cycles. (b) Enlarged XRD patterns between 33° to 38°. (b) Enlarged XRD patterns between 41° to 43°. Arrows indicate shoulders in the XRD peaks due to the formation of the O'3 phase.

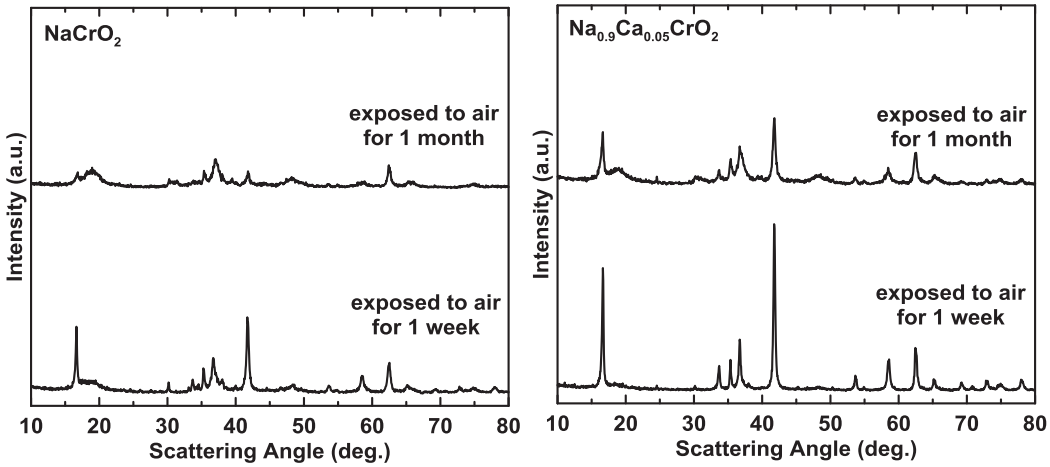

Figure 9. XRD patterns of $NaCrO_2$ and $Na_{0.9}Ca_{0.05}CrO_2$ after air exposure for different durations.

commercialization of sodium ion batteries. The development of air-stable cathode materials therefore is of high importance. Figure 9 shows the XRD patterns of $NaCrO_2$ and $[Na_{0.9}Ca_{0.05}]CrO_2$ after being exposed to room air for one week and one month. After one week, broadened and weakened peaks indicative of structural changes are observed for $NaCrO_2$. Some unidentified impurity peaks are also present. Meanwhile, only slight changes can be observed in the $[Na_{0.9}Ca_{0.05}]CrO_2$ XRD pattern. After 1 month exposure, $NaCrO_2$ becomes almost amorphous and the pristine structure is barely retained, while the XRD profile of $[Na_{0.9}Ca_{0.05}]CrO_2$ only shows broadened and weakened peaks, resembling $NaCrO_2$ after 1 week air exposure. These results suggest that even though calcium substitution cannot eliminate air-sensitivity, the reaction between $Na_{0.9}Ca_{0.05}CrO_2$ and air is mitigated and slowed compared to that of $NaCrO_2$.

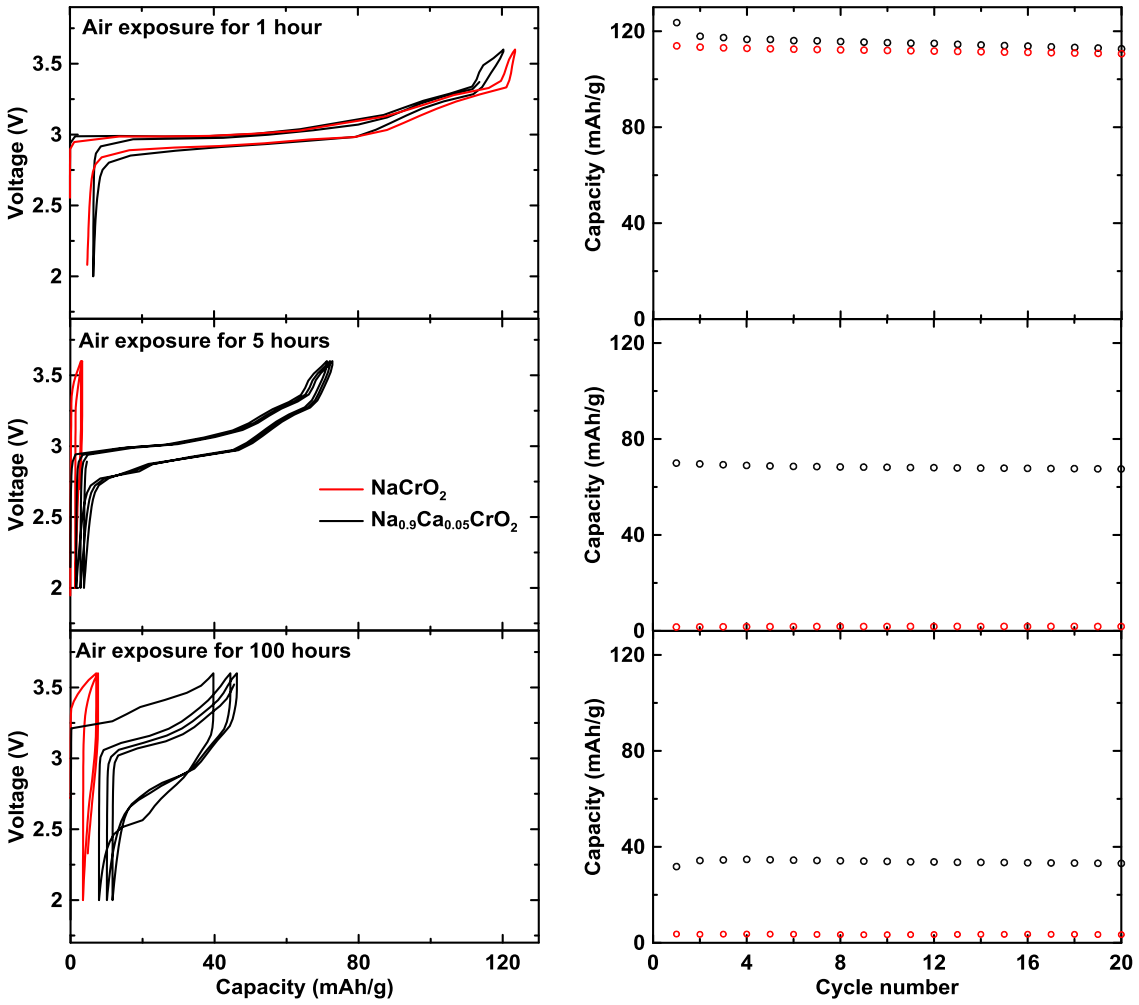

Figure 10. Voltage curves and cycling performance of $NaCrO_2$ and $Na_{0.9}Ca_{0.05}CrO_2$ after air exposure for different durations.

To confirm the improved air stability of calcium substituted $NaCrO_2$, electrochemical tests were conducted. Electrodes were intentionally exposed to air for 1 hour, 5 hours, and 100 hours, and then incorporated into coin cells without any further treatment. It was noticeable to the naked eye that the color of the $NaCrO_2$ electrode quickly changes from black to gray after only several hours of air exposure, while a same color change in the $[Na_{0.9}Ca_{0.05}]CrO_2$ electrodes can only just be observed after a few days of air exposure. The gray color might arise from the formation of $NaOH/Na_2CO_3$ during air exposure. Figure 10 shows voltage curves and the cycling performance of the air-exposed materials. After an hour of air exposure, both materials have identical performance to unexposed materials. However, after 5 hours of air exposure, $NaCrO_2$ become inactive. On the other hand, a reversible capacity of 70 mAh/g was achieved for $[Na_{0.9}Ca_{0.05}]CrO_2$. After 100 hours of air exposure, $[Na_{0.9}Ca_{0.05}]CrO_2$ still retains a capacity of 40 mAh/g. These results confirm the improved air-stability of $[Na_{0.9}Ca_{0.05}]CrO_2$, but also reveals that the slow reaction between the Ca-doped sample and air still occurs. More studies are required to further improve the air-stability.

Conclusions

In summary, calcium doped $Na_{0.9}Ca_{0.05}CrO_2$ was synthesized and its electrochemical and phase behavior investigated. Compared to undoped $NaCrO_2$, $Na_{0.9}Ca_{0.05}CrO_2$ has significantly improved cycling performance and higher coulombic efficiency. The capacity fade rate per cycle of $Na_{0.9}Ca_{0.05}CrO_2$ is only 0.029%, rendering the material an attractive cathode for sodium ion batteries. Ex-situ XRD patterns show that this superior performance can be ascribed to greater structural stability during cycling, possibly due to a stronger calcium-oxygen interaction. Furthermore, both XRD and electrochemical studies show that $Na_{0.9}Ca_{0.05}CrO_2$ also has better air-stability than undoped $NaCrO_2$. It is anticipated that such doping strategies could benefit the development of practical sodium ion batteries cathode materials.

Acknowledgments

The authors acknowledge financial support from NSERC, 3M Canada, the Canada Foundation for Innovation, and the Atlantic Innovation Fund for this work.

ORCID

M. N. Obrovac https://orcid.org/0000-0001-5509-3185

References

1. N. Yabuuchi, K. Kubota, M. Dahbi, and S. Komaba, *Chem. Rev.*, **114**, 11636 (2014).
2. M. D. Slater, D. Kim, E. Lee, and C. S. Johnson, *Adv. Funct. Mater.*, **23**, 947 (2013).
3. M. H. Han, E. Gonzalo, G. Singh, and T. Rojo, *Energy Environ. Sci.*, **8**, 81 (2015).
4. D. A. Stevens and J. R. Dahn, *J. Electrochem. Soc.*, **147**, 1271 (2000).
5. P. Thomas and D. Billaud, *Electrochim. Acta*, **47**, 3303 (2002).
6. S. Komaba, T. Ishikawa, N. Yabuuchi, W. Murata, A. Ito, and Y. Ohsawa, *ACS Appl. Mater. Interfaces*, **3**, 4165 (2011).
7. T. D. Hatchard and M. N. Obrovac, *J. Electrochem. Soc.*, **161**, A1748 (2014).
8. L. Zheng, J. Li, and M. N. Obrovac, *Chem. Mater.*, **29**, 1623 (2017).
9. H. Yoshida, N. Yabuuchi, K. Kubota, I. Ikeuchi, A. Garsuch, M. Schulz-Dobrick, and S. Komaba, *Chem. Commun.*, **50**, 3677 (2014).
10. L. Zheng and M. N. Obrovac, *J. Electrochem. Soc.*, **163**, A2362 (2016).
11. S. Komaba, T. Nakayama, A. Ogata, T. Shimizu, C. Takei, S. Takada, A. Hokura, and I. Nakai, *ECS Trans.*, **16**, 43 (2009).
12. C. Y. Yu, J. S. Park, H. G. Jung, K. Y. Chung, D. Aurbach, Y. K. Sun, and S. T. Myung, *Energy Environ. Sci.*, **8**, 2019 (2015).
13. X. Xia and J. R. Dahn, *Electrochem. Solid-State Lett.*, **15**, A1 (2012).
14. S. Komaba, C. Takei, T. Nakayama, A. Ogata, and N. Yabuuchi, *Electrochem. commun.*, **12**, 355 (2010).
15. K. Kubota, I. Ikeuchi, T. Nakayama, C. Takei, N. Yabuuchi, H. Shiiba, M. Nakayama, and S. Komaba, *J. Phys. Chem. C*, **119**, 166 (2015).
16. S. H. Bo, X. Li, A. J. Toumar, and G. Ceder, *Chem. Mater.*, **28**, 1419 (2016).
17. J. J. Ding, Y. N. Zhou, Q. Sun, and Z. W. Fu, *Electrochem. commun.*, **22**, 85 (2012).
18. Y. Tsuchiya, A. M. Glushenkov, and N. Yabuuchi, *ACS Appl. Nano Mater.*, **1**, 364 (2018).
19. L. Zheng and M. N. Obrovac, *Electrochim. Acta*, **233**, 284 (2017).
20. C. Marino, E. Marelli, and C. Villevieille, *RSC Adv.*, **7**, 13851 (2017).
21. R. Shanmugam and W. Lai, *J. Electrochem. Soc.*, **162**, A8 (2014).
22. D. Buchholz, C. Vaalma, L. Gomes, and S. Passerini, *J. Power Sources*, **282**, 581 (2015).
23. X. Ma, K. Kang, G. Ceder, and Y. S. Meng, *J. Power Sources*, **173**, 550 (2007).
24. X. Zhang, W. J. Jiang, A. Mauger, Qilu, F. Gendron, and C. M. Julien, *J. Power Sources*, **195**, 1292 (2010).
25. M. Matsui, F. Mizukoshi, and N. Imanishi, *J. Power Sources*, **280**, 205 (2015).
26. S. C. Han, H. Lim, J. Jeong, D. Ahn, W. B. Park, K. S. Sohn, and M. Pyo, *J. Power Sources*, **277**, 9 (2015).
27. M. N. Obrovac, T. D. Hatchard, D. S. Iaboni, and U. S. PATENT US 2016/0049653, (2016).
28. R. J. Clément, P. G. Bruce, and C. P. Grey, *J. Electrochem. Soc.*, **162**, A2589 (2015).
29. K. Kubota and S. Komaba, *J. Electrochem. Soc.*, **162**, A2538 (2015).
30. L. Zheng, L. Li, R. Shunmugasundaram, and M. N. Obrovac, *ACS Appl. Mater. Interfaces*, **10**, 38246 (2018).